TRENDS IN SCIENCES 2026; 23(8): 12474
https://doi.org/10.48048/tis.2026.12474
RESEARCH ARTICLE

High Saturated-Magnetization-Realization Induced by Zinc Substitution in Cobalt Ferrite Nanoparticles Synthesized via Sol-Gel Method

Nurdiyantoro Putra Prasetya[1,2], Siti Nurjanah[2], Retna Arilasita[1], Utari[2], Riyatun[2], Suharno[3], Suharyana[2] and Budi Purnama[2,*]

[1]Department of Physics, Faculty of Mathematics and Natural Sciences, Universitas Tanjungpura, Pontianak 78124, Indonesia
[2]Department of Physics, Faculty of Mathematics and Natural Sciences, Universitas Sebelas Maret, Surakarta 57126, Indonesia
[3]Department of Physics Education, Faculty of Teacher Training and Education, Universitas Sebelas Maret, Surakarta 57126, Indonesia

([*]Corresponding author's e-mail: bpurnama@mipa.uns.ac.id)

Received: 31 October 2025, Revised: 31 December 2025, Accepted: 20 January 2026, Published: 20 March 2026

Abstract

Cobalt ferrite ($CoFe_2O_4$) is a promising spinel ferrite material due to its high chemical stability, moderate saturation magnetization, and significant coercivity, making it attractive for various technological applications such as magnetic data storage, sensors, and photocatalysis. Tailoring its properties via cationic substitution enables precise tuning of both structural and magnetic characteristics. In this study, zinc-substituted cobalt ferrite nanoparticles with Zn^{2+} concentrations of x = 0, 0.2 and 0.4 were synthesized via the sol-gel method and thermally annealed at 450 °C for 6 h. X-ray diffraction (XRD) patterns confirmed a single-phase face-centered cubic spinel structure (space group Fd-3m), corroborated by Rietveld refinement. FTIR spectra revealed characteristic vibrational bands at tetrahedral (ν_1) and octahedral (ν_2) sites, confirming spinel formation. Magnetic measurements showed a significant reduction in coercivity from 1,130 Oe (x = 0) to 247 Oe (x = 0.4), attributed to a domain transition from single- to multi-domain structure. Meanwhile, saturation magnetization increased from 75.77 to 104.74 emu/g, linked to the redistribution of non-magnetic Zn^{2+} ions to tetrahedral sites, replacing magnetic Co^{2+}, and the migration of Fe^{3+} to octahedral positions. Additionally, the emergence of spin reverse-orientation of Fe^{3+} at tetrahedral sublattice contributed to the enhancement in magnetization. These interpretations were further supported by magnetic structure simulations using the BasIreps program, confirming the presence of spin-down ordering in trivalent cation of tetrahedral site. This study provides insights into Zn's role in modulating the magneto-structural behavior of cobalt ferrite for advanced magnetic materials.

Keywords: Cobalt ferrite, Zinc, Sol-gel, Spinel structure, Single-domain, Multi-domain, Saturation magnetization, Spin reverse-orientation

Introduction

Spinel ferrites have attracted tremendous attention in the last decades owing to their remarkable structural versatility and tunable magnetic properties [1,2], which make them suitable for a wide spectrum of technological applications, including magnetic data storage [3], ferrofluids [4], microwave devices [5], catalysis [6], and biomedical fields [7]. Among them, cobalt ferrite ($CoFe_2O_4$) has been recognized as a particularly promising material due to its high chemical stability, significant coercivity, moderate saturation magnetization, and mechanical hardness [8]. These features position cobalt ferrite as a candidate for multifunctional applications where both durability and magnetic performance are crucial.

One of the most effective approaches to tailor the structural and magnetic properties of cobalt ferrite is cationic substitution at tetrahedral (A) or octahedral (B) sites within the spinel lattice [9,10]. Such substitutions can induce profound modifications in cation distribution, exchange interactions, and spin alignment, thereby altering the overall magneto-structural behavior. In this context, zinc (Zn^{2+}) substitution has been widely explored because of its strong site preference for tetrahedral coordination and its non-magnetic nature [11-14]. The introduction of Zn^{2+} ions into $CoFe_2O_4$ is expected to displace magnetic Co^{2+} ions from tetrahedral to octahedral sites, which in turn modifies the superexchange interactions between Fe^{3+} ions across A and B sites [15]. This redistribution mechanism not only governs the balance between ferromagnetic and antiferromagnetic contributions but also directly impacts domain structure evolution.

Previous studies have reported that zinc incorporation generally enhances saturation magnetization while reducing coercivity, which is beneficial for soft magnetic applications [16-18]. However, the underlying microscopic mechanism, particularly the emergence of antiferromagnetic (especially spin-down) ordering within the tetrahedral sublattice, remains insufficiently clarified. Most reports primarily address macroscopic magnetic measurements without combining them with structural refinements and magnetic symmetry analysis, which are essential to unambiguously establish the correlation between cation redistribution and magnetic ordering.

On the other hand, synthesis is a crucial step in modulating the structural phenomena and functional properties of $CoFe_2O_4$ nanoparticles, so that the regulation of thermal conditions, especially the synthesis temperature and annealing temperature, is an aspect that cannot be ignored. The study reported by Fatimah *et al.* [19] on Zn-substituted $CoFe_2O_4$ nanoparticles showed through TG-DTA analysis that the precursor decomposition process and the formation of a stable spinel phase began to be achieved at a temperature of around 400 °C. This finding indicates that this temperature is sufficient to produce initial thermal stability, but still requires further treatment to improve crystallinity. Therefore, in this study an annealing temperature of 450 °C was chosen, which is expected to encourage the development of a better crystal structure without causing excessive particle growth or undesirable phase changes.

In this study, the structural and magnetic behavior of zinc-substituted cobalt ferrite nanoparticles synthesized via the sol-gel method was systematically investigated. X-ray diffraction combined with Rietveld refinement and FTIR spectroscopy was employed to confirm phase purity and spinel formation. Magnetic measurements, supported by magnetic structure simulations using the BasIreps program, provide insights into the spin configuration induced by Zn^{2+} substitution, particularly at tetrahedral and octahedral sites. This work contributes to a deeper understanding of the role of zinc in modulating cation distribution, which supports the orientation of the magnetic moment in cobalt ferrites, offering valuable guidelines for designing advanced soft magnetic materials with controllable properties.

Materials and methods

Materials

Analytical grade ferric nitrate nonahydrate ($Fe(NO_3)_3 \cdot 9H_2O$), cobalt nitrate hexahydrate ($Co(NO_3)_2 \cdot 6H_2O$), zinc nitrate hexahydrate ($Zn(NO_3)_2 \cdot 6H_2O$), and citric acid ($C_6H_8O_7$) were obtained from Merck (≥ 99% purity) and used without further purification. Deionized water was employed as the solvent throughout the synthesis process. Zinc concentrations were varied with substitution levels of x = 0.0, 0.2, and 0.4 in $Zn_xCo_{1-x}Fe_2O_4$.

Synthesis of Zn-substituted cobalt ferrite nanoparticles

Zinc-substituted cobalt ferrite nanoparticles were synthesized via a modified sol-gel method. Stoichiometric amounts of $Fe(NO_3)_3 \cdot 9H_2O$, $Co(NO_3)_2 \cdot 6H_2O$ and $Zn(NO_3)_2 \cdot 6H_2O$ (according to the desired composition) were dissolved in deionized water under continuous magnetic stirring. Citric acid was introduced as a chelating agent to promote gel formation.

The homogeneous solution was stirred for 5 min and subsequently heated to 90 °C until a gel-like structure was formed. The resulting viscous gel was

subjected to hydrolysis at 100 °C until a dry precursor was obtained. The dried precursor was manually ground to ensure homogeneity before being annealed at 450 °C for 6 h in a muffle furnace. After annealing, the powder was reground to achieve uniform particle size and homogeneity, yielding the final $Zn_xCo_{1-x}Fe_2O_4$ nanoparticles (**Figure 1**).

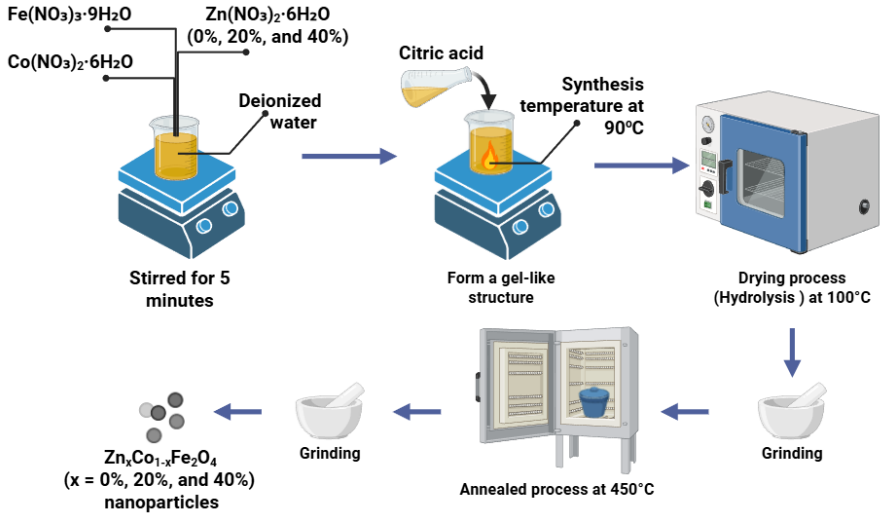

Figure 1 Schematic of the synthesis of Zinc-substituted $CoFe_2O_4$ nanoparticles by sol-gel method.

Characterization techniques

The structural, vibrational, and magnetic properties of the synthesized nanoparticles were comprehensively characterized. Structural analysis was carried out using X-ray diffraction (XRD, PanAnalytical X'Pert Pro, Cu-Kα, λ = 1.5406 Å) combined with Rietveld refinement to determine lattice parameters, crystallite size, and phase composition. Additionally, Crystallite size (D) was calculated by the Debye-Scherrer equation via the hkl (311) strongest peak, which was the result used for determining lattice strain (ε), lattice parameter (a_{cal}), and density (d_x) from XRD results. The parameters of the XRD results were calculated as follows [20-22]:

$$D = \frac{0.9\lambda}{\beta cos\theta} \quad (1)$$

$$\varepsilon = \frac{\beta}{4tan\theta} \quad (2)$$

$$a_{cal} = d_{hkl}\sqrt{h^2 + k^2 + l^2} \quad (3)$$

$$d_x = \frac{8M}{N_A a_{cal}{}^3} \quad (4)$$

where λ is the wavelength of the Cu-Kα source, β is the full width at half maximum (FWHM), θ is the Bragg diffraction angle, d_{hkl} is the distance between the planes, M is the molecular weight, and N_A is Avogadro's number.

Fourier transform infrared (FTIR) spectroscopy (Shimadzu IR Prestige 21) in the range of 400 - 4,000 cm^{-1} was employed to identify metal-oxygen bonding and confirm spinel formation. Magnetic measurements were performed using a vibrating sample magnetometer (VSM, Oxford VSM 1.2H) at room temperature with an applied magnetic field ranging from –10 to +10 kOe to evaluate coercivity (Hc), saturation magnetization (Ms), and remanence (Mr). On the other hand, VSM results were also used for determining magnetic moment (n_B) and magnetocrystalline anisotropy (K), as follows [10]:

$$n_B = \frac{M \times M_S}{5585} \quad (5)$$

$$K = \frac{H_C \times M_S}{0.96} \quad (6)$$

For support of VSM analysis, magnetic structure simulations were conducted using the BasIreps

program to elucidate further spin-reverse orientation ordering induced by Zn substitution.

Results and discussion

The X-ray diffraction (XRD) patterns presented in **Figure 2** confirm that all $Zn_xCo_{1-x}Fe_2O_4$ samples with different Zn concentrations (x = 0, 0.2 and 0.4) crystallize in a cubic spinel (FCC) structure with the *Fd-3m* space group, in agreement with the ICDD 22-1086 database [13,23]. The most intense diffraction peak is observed for the (311) plane, which is the characteristic orientation of the spinel phase. This finding indicates that Zn^{2+} substitution into the crystal lattice does not alter the primary phase, but modifies the lattice parameter and microstructural characteristics through cation redistribution between tetrahedral and octahedral sites.

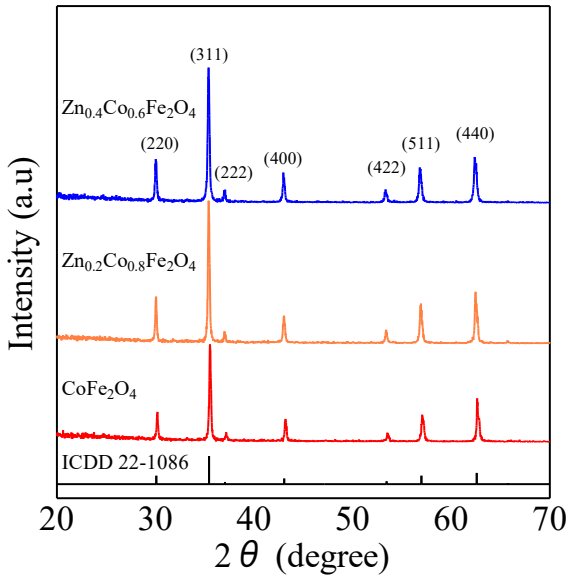

Figure 2 XRD Pattern of $Zn_xCo_{1-x}Fe_2O_4$ nanoparticles (x = 0.0, 0.2 and 0.4) by sol-gel method.

The Rietveld refinement results (**Figure 3** and **Table 1**) further support this observation, where the experimental diffraction data are well-fitted with a single spinel phase model. The low goodness of fit (χ^2) magnitude, which is close to 1, together with the reliability factors (R_p, R_{wp}, R_{exp}), demonstrate the consistency of the refined structural model with the experimental data [10,24]. Moreover, the lattice parameter (a) increases progressively with higher Zn concentration, which can be explained by the difference in ionic radii between Zn^{2+} (0.60 Å, tetrahedral site) and Co^{2+} (0.90 Å, octahedral site) [25]. This substitution induces local distortions, leading to lattice expansion. Such a trend is consistent with previous reports on Zn-substituted ferrites, where redistribution of cations within the spinel structure results in similar unit cell enlargement [26].

Furthermore, the calculated crystallite size (D), lattice parameter (a_{cal}), theoretical density (d_x), and lattice strain (ε), as shown in **Table 2** [10], reveal the significant effect of Zn substitution. The crystallite size, D, decreases with increasing Zn content, while the lattice strain, ε, increases (**Figure 4**). The reduction in crystallite size is associated with the inhibitory role of Zn^{2+} in grain growth, owing to enhanced lattice distortions [26]. In contrast, the increase in lattice strain is attributed to internal relaxation and structural imperfections induced by cation substitution [24]. The increase in the calculated lattice parameter, a_{cal}, is consistent with the refinement results, which can be explained by the difference in ionic radii between Zn^{2+} and Co^{2+}, leading to local distortions that result in lattice parameter expansion [27]. These findings collectively imply that Zn substitution enhances internal lattice stress and encourages more refined recrystallization, both of which are anticipated to impact the material's functional characteristics.

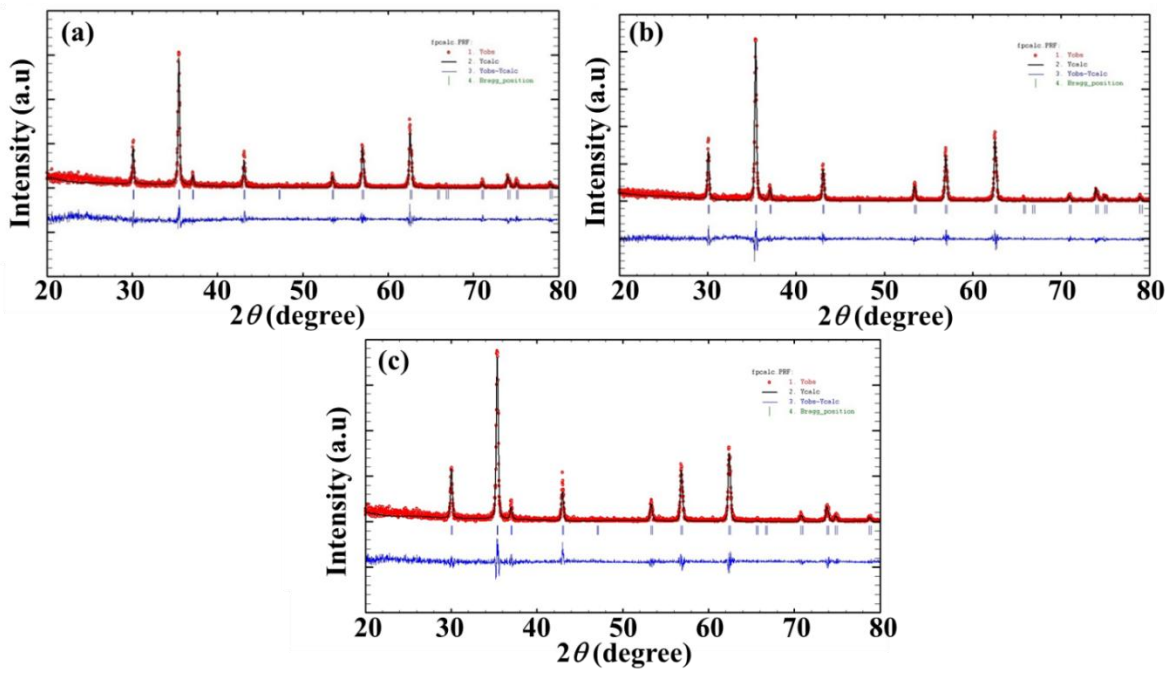

Figure 3 Rietveld refinement on XRD results for $Zn_xCo_{1-x}Fe_2O_4$ nanoparticles (x = (a) 0%, (b) 20%, and (c) 40%) by sol-gel method.

Table 1 The rietveld analysis parameters at crystal system cubic and space group Fd-3m of the samples S1, S2 and S3 (S1 = $CoFe_2O_4$, S2 = $Co_{0.8}Zn_{0.2}Fe_2O_4$, S3 = $Co_{0.6}Zn_{0.4}Fe_2O_4$).

Structural	The samples		
	S1	**S2**	**S3**
R_p	43.50	39.20	38.80
R_{wp}	51.60	47.50	42.80
R_{exp}	42.30	37.70	38.60
R_F	19.90	16.90	16.70
R_B	18.28	12.60	11.98
χ^2	1.49	1.60	1.56
a, b, c (Å)	8.38980	8.39710	8.41240
α, β, γ	90.0000	90.0000	90.0000
Co			
x	0.00000	0.00000	0.00000
y	0.00000	0.00000	0.00000
z	0.00000	0.00000	0.00000
Fe			
x	0.62500	0.62500	0.62500
y	0.62500	0.62500	0.62500
z	0.62500	0.62500	0.62500
O			
x	0.38000	0.38210	0.38320
y	0.38000	0.38210	0.38320
z	0.38000	0.38210	0.38320

Hence, Zn substitution in cobalt ferrite is a key factor in altering the structural characteristics, as demonstrated by the combined evidence from XRD patterns, Rietveld refinement, and crystallographic parameter analysis. These structural changes offer chances to customize the material's functional characteristics through regulated cation substitution and confirm the stability of the single-phase spinel.

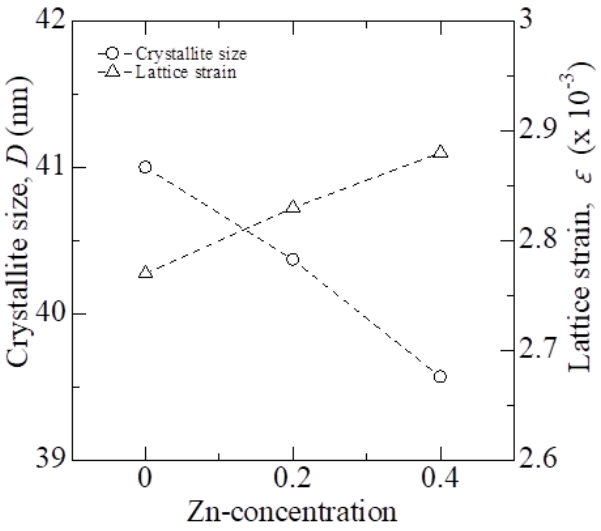

Figure 4 The effect of Zn concentration on crystallite size and lattice strain of cobalt ferrite nanoparticles.

Table 2 Crystallite size (D), lattice strain (ε), lattice parameter (a_{cal}), and density (d_x) of $Zn_xCo_{1-x}Fe_2O_4$ nanoparticles (x = 0.0, 0.2 and 0.4) by sol-gel method.

x	D (nm)	ε ($\times 10^{-3}$)	a_{cal} (Å)	d_x (gr/cm^3)
0	41.00	2.77	8.384	5.288
0.2	40.37	2.83	8.416	5.256
0.4	39.57	2.88	8.416	5.285

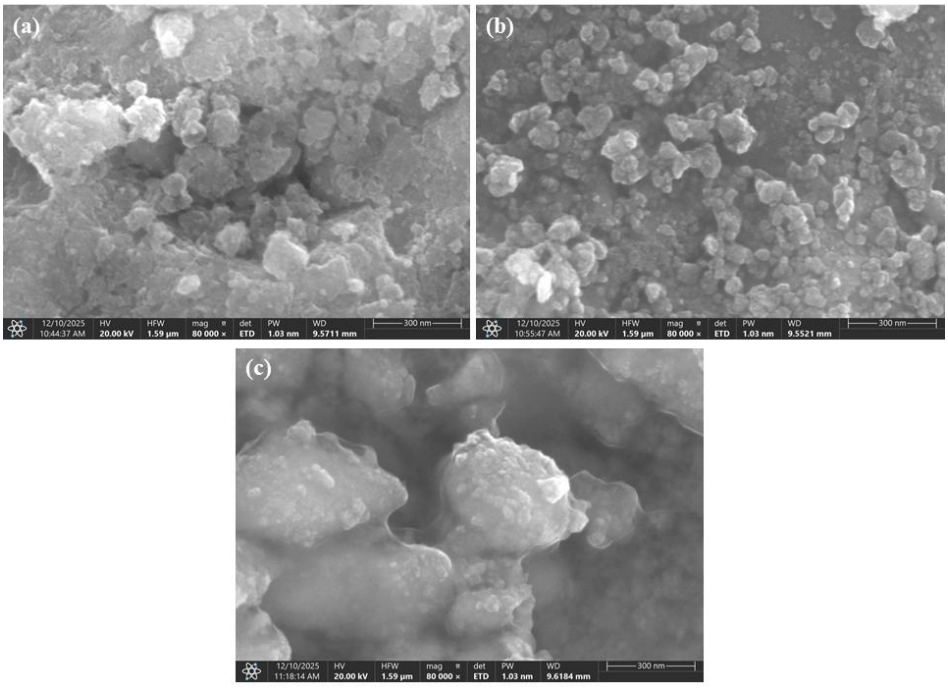

Figure 5 The morphology of cobalt ferrite nanoparticles with Zn substitution of (a) 0%, (b) 20%, and (c) 40%.

Figure 5 presents the SEM images of cobalt ferrite nanoparticles with varying Zn substitution levels. The pristine sample (Zn = 0%) exhibits irregularly shaped nanoparticles with pronounced agglomeration, which is commonly attributed to strong magnetic dipole-dipole interactions inherent to cobalt ferrite nanoparticles. These interactions promote particle clustering, resulting in dense and compact agglomerates. Upon substitution of 20% Zn, a noticeable change in morphology is observed. The particles appear relatively more dispersed with reduced agglomeration, although clustering is still present. This behavior can be attributed to the partial replacement of magnetic Co^{2+} ions by non-magnetic Zn^{2+} ions, which weakens interparticle magnetic interactions and suppresses excessive particle coalescence during synthesis. At higher Zn substitution (40%), the nanoparticles tend to form larger, loosely connected aggregates with smoother surfaces. This morphology suggests enhanced particle growth and coalescence, likely driven by lattice expansion and modified cation distribution within the spinel structure. The incorporation of larger Zn^{2+} ions alters nucleation and growth kinetics, leading to increased particle size and the formation of more compact secondary structures [28]. In addition, **Figure 5** illustrates the morphological evolution of cobalt ferrite nanoparticles with increasing Zn substitution. The undoped sample (Zn = 0%) consists of relatively small, strongly agglomerated nanoparticles, which are characteristic of the single-domain regime, where strong dipole-dipole interactions dominate. At 20% Zn substitution, particle dispersion improves, and agglomeration is reduced, indicating weakened magnetic interactions and the stabilization of single-to multi-domain behavior due to decreased magnetic anisotropy. At higher Zn content (40%), larger particles and secondary aggregates are formed, favoring the development of multi-domain structures, where domain wall formation becomes energetically favorable. This single-to multi-domain transition correlates well with the observed changes in magnetic properties discussed in the subsequent section.

Figure 6 displays the FTIR spectra of $Zn_xCo_{1-x}Fe_2O_4$ (x = 0, 0.2 and 0.4), exhibiting the 2 typical spinel bands: ν_1 (tetrahedral M–O stretching) at ~587 - 575 cm^{-1} and ν_2 (octahedral M–O stretching) at ~399 cm^{-1} [29,30]. The presence of these bands in all compositions confirms the preservation of the spinel framework, consistent with the XRD/Rietveld results indicating a single-phase structure with space group Fd-3m. Notably, ν_1 shows a systematic red shift with increasing Zn content (587.35 → 581.56 → 574.81 cm^{-1}), whereas ν_2 band remains nearly unchanged (≈ 399.3 cm^{-1}). This behavior is consistent with the strong preference of Zn^{2+} for occupying tetrahedral sites, which more significantly influences the local A-site environment compared to the B-site, while maintaining the stability of the overall spinel lattice.

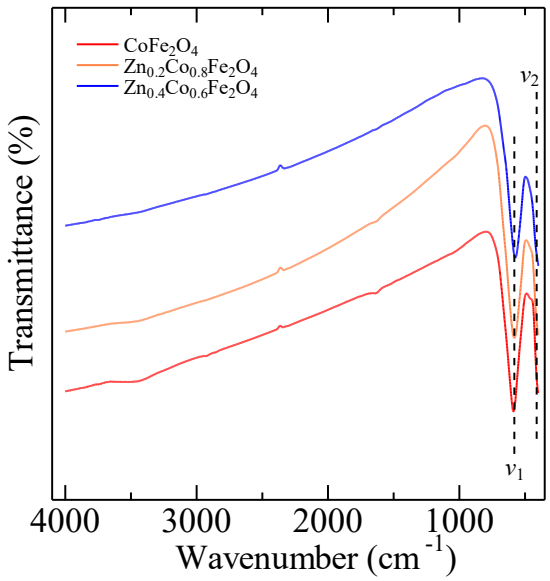

Figure 6 FTIR spectra of $Zn_xCo_{1-x}Fe_2O_4$ nanoparticles (x = 0.0, 0.2 and 0.4) by sol-gel method.

The red shift of the v_1 band can be explained by 2 main effects. First, the effective reduced mass, μ, of the tetrahedral M–O pair increases when the heavier Zn^{2+} replaces Co^{2+}, thereby lowering the vibrational frequency for a given force constant $\left(v \propto \sqrt{k/\mu}\right)$ [29]. Second, cation redistribution ($Zn^{2+} \rightarrow$ A; Co^{2+}, $Fe^{3+} \rightarrow$ B) together with the lattice expansion detected by XRD induces local distortions and slightly elongates the tetrahedral M–O bond length, further enhancing the red shift. Conversely, the stability of the v_2 band indicates that the average B-site environment remains largely unaffected despite the migration of Co^{2+}/Fe^{3+}.

The calculated force constants (**Table 3**) reveal a slight increase in the tetrahedral constant k_t (146.80 → 148.84 → 150.20 N/m), accompanied by a small decrease in the octahedral constant k_o (97.14 → 96.62 → 96.10 N/m). Considering the relation $v \propto \sqrt{k/\mu}$, the increase in μ due to Zn substitution at the A-site offsets—and even dominates—the modest strengthening of k_t, thus producing the observed red shift of v_1. The slight reduction in k_o suggests subtle relaxation in the B-site network as Fe^{3+} becomes more dominant, consistent with lattice expansion and strain observed in the XRD results [31-33]. Consequently, the v_1/v_2 shifts and the k_t/k_o trends complement the crystallographic image of cation redistribution derived from XRD/Rietveld analysis and offer spectroscopic proof of Zn^{2+} inclusion at the tetrahedral locations.

Table 3 FTIR parameters of $Zn_xCo_{1-x}Fe_2O_4$ nanoparticles (x = 0.0, 0.2 and 0.4) by sol-gel method.

x	v_1 (cm^{-1})	v_2 (cm^{-1})	k_t (N/m)	k_o (N/m)
0	587.35	399.28	146.80	97.14
0.2	581.56	399.28	148.84	96.62
0.4	574.81	399.28	150.20	96.10

Figure 7 shows the M–H hysteresis curves of $Zn_xCo_{1-x}Fe_2O_4$ (x = 0, 0.2 and 0.4), and **Table 4** lists the corresponding magnetic parameters. The data indicate changes in the magnetic properties with increasing Zn concentration, which are associated with cation redistribution, domain structure, and magnetocrystalline anisotropy.

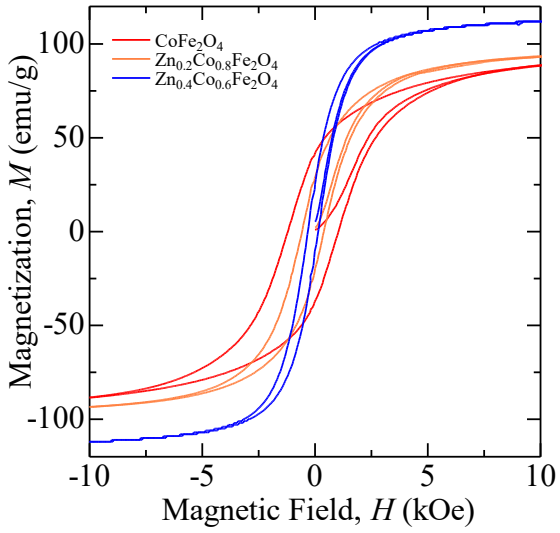

Figure 7 M–H hysteresis curve of $Zn_xCo_{1-x}Fe_2O_4$ nanoparticles (x = 0.0, 0.2 and 0.4) by sol-gel method.

The coercivity (Hc) decreases significantly from 1,130 Oe (x = 0) to 247 Oe (x = 0.4), indicating a transition from a single-domain (SD) to a multi-domain (MD) state. This trend is characteristic of a reduction in magnetocrystalline anisotropy (K) due to the incorporation of Zn^{2+} ions. Since Zn^{2+} is non-magnetic and preferentially occupies tetrahedral (A) sites, the A–B superexchange interaction is weakened, making the

system soft magnetic and reducing anisotropy barriers. The decline in the squareness ratio (Mr/Ms) from 0.52 to 0.17 further supports the SD → MD transition, consistent with cation redistribution and spin canting effects within the B sublattice [34,35].

In contrast to the coercivity trend, the saturation magnetization (Ms) increases steadily from 75.77 emu/g (x = 0) to 104.77 emu/g (x = 0.4). This enhancement can be explained within the Néel model [36], where the net magnetic moment arises from the difference between the octahedral (B) and tetrahedral (A) sublattices ($Ms = M_B - M_A$) [37,38]. Additionally, the results are supported by BasIreps data results, which emphasize the magnetic configuration opposite to pristine $CoFe_2O_4$, which allows the possibility of octahedral and tetrahedral magnetic moment orientation in the same direction/aligned with increasing Zn value, which plays a role in rotating the orientation of the magnetic moments. The substitution of non-magnetic Zn^{2+} ions into the A-sites drives the migration of magnetic Fe^{3+}/Co^{2+} ions to the B-sites. As a result, the magnetic moment at the B sublattice increases, strengthening the B–O–B superexchange interaction and thereby enhancing M_B. Consequently, higher Zn concentrations yield larger Ms magnitudes. The observed increase in Ms is consistent with XRD results showing lattice parameter expansion due to cation redistribution and FTIR data indicating local distortions through vibrational frequency shifts.

The effective magnetic moment (n_B) increases from 3.18 μ_B (x = 0) to 4.45 μ_B (x = 0.4), supporting the notion of enhanced total magnetic moments induced by cation redistribution. These results also support the presence of the highest saturation magnetization (104.77 emu/g) with 40% Zn concentration, consistent with a previous study that shows an increase in saturation magnetization with 0.4 concentration, after which there is a decreasing tendency above 0.4 concentration [12,39]. Conversely, the magnetocrystalline anisotropy constant (K) decreases significantly from 4.62×10^5 to 1.40×10^5 erg/cm^3, confirming that the system becomes soft magnetic close to superparamagnetic (x = 0.4) [40]. The strong correlation between the reduction in Hc, Mr/Ms, and K with the enhancement in Ms and n_B demonstrates that Zn substitution produces ferrite materials with high saturation magnetization but low coercivity.

Thus, the magnetic results show that Zn substitution efficiently modifies the structural and magnetic environment of $CoFe_2O_4$, encourages cation redistribution, and produces materials with low Hc and high Ms. Applications in microwave absorbers, spintronic components, and electromagnetic devices—where soft magnetic behavior with increased saturation magnetization is essential—benefit greatly from these properties.

Table 4 Magnetic parameters of $Zn_xCo_{1-x}Fe_2O_4$ nanoparticles (x = 0.0, 0.2 and 0.4) by sol-gel method.

x	Hc (Oe)	Ms (emu/g)	Mr (emu/g)	Mr/Ms	n_B (μ_B)	K ($\times10^5$) (erg/cm^3)
0	1,130	75.77	39.75	0.52	3.18	4.62
0.2	470	85.76	24.00	0.28	3.62	2.16
0.4	247	104.74	17.85	0.17	4.45	1.40

Rietveld refinement analysis indicates that cobalt ferrite ($CoFe_2O_4$) crystallizes with a lattice parameter of 8.3898 Å, with Fe atoms located at fractional coordinates (x,y,z) = (0.6250, 0.6250, 0.6250). Upon Zn substitution, the lattice parameter systematically expands to 8.3971 Å for 20% Zn and 8.4124 Å for 40% Zn. This expansion is attributed to the larger ionic radius of Zn^{2+} (0.60 Å) compared with Co^{2+} (0.56 Å). In accordance with the spinel cation distribution, Zn^{2+} preferentially occupies the tetrahedral (A) sites, replacing Co^{2+} ions, which are predominantly located in the octahedral (B) sites of the inverse spinel structure. Meanwhile, Fe^{3+} ions are distributed over both A- and B-sites, playing a central role in mediating the overall magnetic interactions.

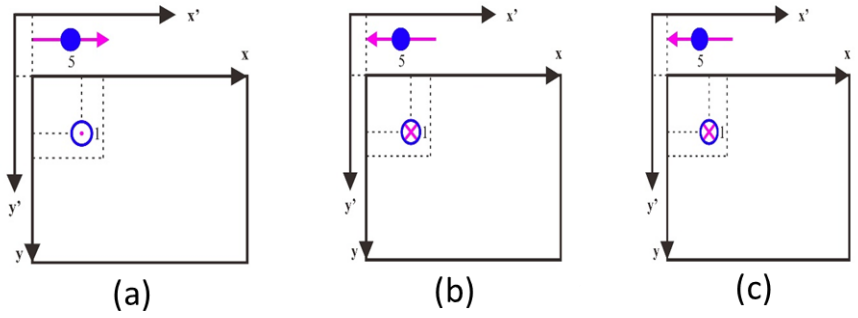

Figure 8 Possible spin orientations of Fe_1 atoms: (a) oriented out of the z-plane in $CoFe_2O_4$, (b) oriented into the z-plane in $Zn_{0.2}Co_{0.8}Fe_2O_4$, and (c) oriented into the z-plane in $Zn_{0.4}Co_{0.6}Fe_2O_4$.

Simulation results obtained using the BasIreps program [41] (following $O_s\Gamma_v = \sum_\mu \Gamma_\mu R_{\mu v}(S)$ for $\Gamma = \sum_{i=1}^{n(v)} \Gamma_i$) with the cubic space group Fd-3m reveal systematic changes in the spin orientations of Fe atoms upon Zn substitution. In pristine $CoFe_2O_4$, Fe_1 atoms exhibit a spin orientation of (1,1,1), while Fe_5 atoms show a spin orientation of (1,1,−1). At 20% Zn substitution, the spin orientation of Fe_1 changes to (1,1,−1), whereas Fe_5 adopts (−1,1,−1). At 40% Zn, these orientations become more stabilized, indicating a tendency toward an antiferromagnetic arrangement (rising spin-down orientation) compared to the pristine sample.

The spin configuration visualizations (**Figure 8**) further support this interpretation. In pure $CoFe_2O_4$, Fe_1 spins tend to orient outside the z-plane. At 20% Zn substitution, Fe_1 spins shift into the z-plane, while at 40% Zn they become more firmly stabilized along this axis. This behaviour can be explained by the non-magnetic nature of Zn^{2+} at the tetrahedral sites, which weakens the superexchange interaction between Fe^{3+}(A)–O^{2-}–Fe^{3+}(B). Consequently, the contribution of Fe^{3+}(B)–O^{2-}–Fe^{3+}(B) interactions within the octahedral sublattice becomes dominant, leading to the experimentally observed increase in saturation magnetization (Ms). These results confirm that Zn can rotate the orientation of the magnetic moment in the spinel ferrite structure, so that the greater the quantity of Zn, the greater the magnetic configuration that is opposite to pristine $CoFe_2O_4$.

In addition, Zn^{2+} substitution in the $CoFe_2O_4$ lattice induces a measurable lattice expansion due to the larger ionic radius of Zn^{2+} compared to Co^{2+}, which in turn alters the local crystal field environment of neighboring Fe^{3+} ions. As illustrated schematically in **Figure 9**, the preferential occupation of Zn^{2+} at tetrahedral sites triggers a redistribution of Fe^{3+} cations toward octahedral sites, leading to a reorientation of Fe spin moments, particularly at the Fe_1 and Fe_5 positions. This spin reorganization modifies the balance between antiparallel sublattices and enhances intra-octahedral (B–B) magnetic interactions, which become more dominant as the Zn content increases. Consequently, the reduction in magnetic moment at the tetrahedral sublattice and the stabilization of spin alignment within the octahedral sublattice contribute to the observed increase in saturation magnetization (Ms), establishing a clear correlation between lattice expansion, cation redistribution, spin reorientation, and magnetic enhancement in Zn-substituted $CoFe_2O_4$ nanoparticles.

Overall, the distribution of Zn^{2+} ions in the tetrahedral sites, Co^{2+} ions in the octahedral sites, and Fe^{3+} ions across both tetrahedral and octahedral sites provides a consistent explanation for the structural expansion, spin reorientation, and enhanced magnetic properties. Zn substitution thus promotes lattice expansion, modifies Fe^{3+} spin alignment, and strengthens intra-octahedral magnetic interactions, in agreement with the observed rise in Ms magnitudes.

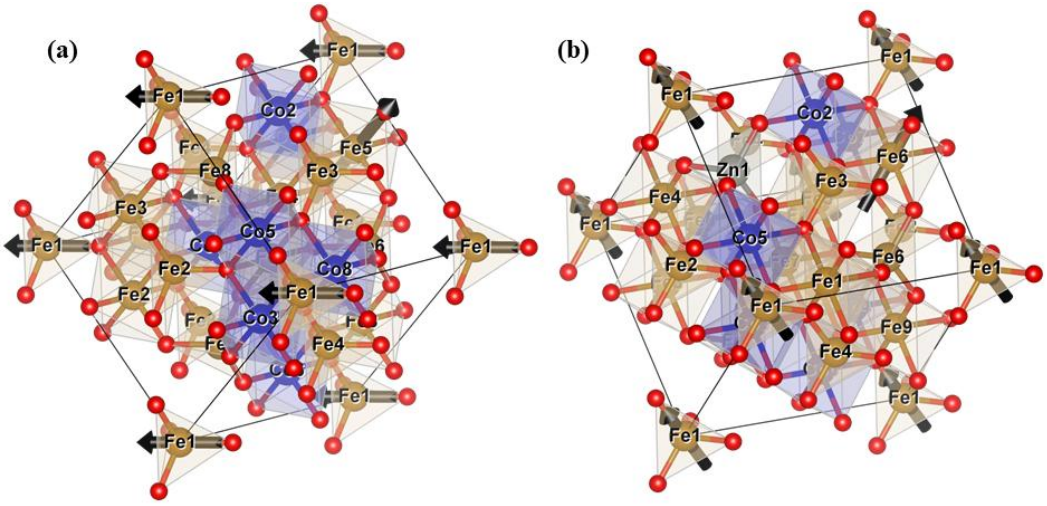

Figure 9 Illustration of the orientation magnetic moment in cobalt ferrite nanoparticles at Fe1 and Fe5 atoms of (a) without and (b) with Zn substitution.

Conclusions

Cobalt ferrite nanoparticles substituted with zinc ($Zn_xCo_{1-x}Fe_2O_4$, x = 0, 0.2 and 0.4) were successfully synthesized via the sol-gel method followed by annealing at 450 °C for 6 h. XRD characterization confirmed that all samples crystallized in a cubic spinel (FCC) structure with space group Fd-3m, consistent with ICDD 22-1086. FTIR analysis further verified the presence of characteristic absorption bands at the tetrahedral (v_1) and octahedral (v_2) sites, supporting the structural stability of the spinel phase. Magnetic measurements revealed a decrease in coercivity (Hc) and an increase in saturation magnetization (Ms) with higher Zn content, attributed to Zn^{2+} occupation at tetrahedral sites, which weakens A–B superexchange while enhancing B–B interactions. BasIreps simulations complemented these findings by showing spin reverse-orientation of Fe atoms and a tendency toward spin-down ordering of trivalent cation in the tetrahedral site with Zn substitution. Overall, the results demonstrate that Zn substitution effectively modifies the structural and magnetic properties of cobalt ferrite, making it a promising material for spinel-based magnetic and photocatalytic applications.

Acknowledgements

This study was financially supported by Penguatan Kapasitas Grup Riset (PKGR-UNS) A Universitas Sebelas Maret, Indonesia contract number: 371/UN27.22/PT.01.03/2025.

Declaration of generative AI in scientific writing

The authors acknowledge the use of generative AI tools (Grammarly) in the preparation of this manuscript, specifically for language editing and grammar correction. No content generation or data interpretation was performed by AI. The authors take full responsibility for the content and conclusions of this work.

CRediT author statement

Nurdiyantoro Putra Prasetya: Writing - Original Draft; Investigation; Formal analysis. **Siti Nurjanah**: Methodology; Formal analysis. **Retna Arilasita**: Data Curation; Formal analysis. **Utari**: Supervision; Validation. **Riyatun**: Supervision; Project administration. **Suharno**: Software; Validation. **Suharyana**: Formal analysis. **Budi Purnama**: Conceptualization; Funding acquisition; Writing - Review & Editing; Supervision.

References

[1] A Akbar, M Bhavani Lakshmi, TK Das and M Ghosh. Spinel ferrites in the photocatalytic and adsorptive remediation of dyes and heavy metals: A review. *Journal of Water Process Engineering* 2025; **71**, 107259.

[2] FM Zulhaina, NP Prasetya, Riyatun, Utari and B Purnama. Silver content modification of structural, magnetic and antibacterial properties in magnetite nanoparticles. *Trends in Sciences* 2025; **22(3)**, 9182.

[3] A Ahmed, M Khalid, MGB Ashiq, I Boukhris, M Younas, W Ullah, MS Al-Buriahi, K Naz, MA Siddique and M ul Haq. Praseodymium doped Ni-Co based spinel ferrite nanoparticles prepared for energy storage applications. *Physica B: Condensed Matter* 2025; **700**, 416947.

[4] M Dinarvand, M Abolhasani, F Hormozi and Z Bahrami. Experimental investigation and performance comparison of Fe_3O_4/water and $CoFe_2O_4$/ water ferrofluids in presence of a magnetic field in a cooling system *Journal of the Taiwan Institute of Chemical Engineers* 2023; **148**, 104927.

[5] K Naz, JK Khan, M Khalid, MS Akhtar, ZA Gilani, HM Noor ul Huda Khan Asghar, GAM Mersal, MM Ibrahim, A Muhammad and MGB Ashiq. Structural, dielectric, impedance and electric modulus analysis of Ni substituted copper spinel ferrites nanoparticles for microwave device applications. *Materials Chemistry and Physics* 2022; **285**, 126091.

[6] H Qin, Y He, P Xu, D Huang, Z Wang, H Wang, Z Wang, Y Zhao, Q Tian and C Wang. Spinel ferrites (MFe_2O_4): Synthesis, improvement and catalytic application in environment and energy field. *Advances in Colloid and Interface Science* 2021; **294**, 102486.

[7] EF Esmer, E Bilgi, SÇ Dincay, T Sakallı and CÖ Karakuş. Design, synthesis, characterization and biological evaluation of cobalt-ferrite nanoparticles for biomedical applications. *Journal of Magnetism and Magnetic Materials* 2025; **629**, 173336.

[8] QY Tamboli, SM Patange, YK Mohanta, R Sharma and KR Zakde. Green synthesis of cobalt ferrite nanoparticles: an emerging material for environmental and biomedical applications. *Journal of Nanomaterials* 2023; **2023(1)**, 9770212.

[9] YS Bopche, AM Shahare, DS Choudhary and AV Bagde. A brief review on structural, morphological, magnetic and dielectric behavior of divalent cation-substituted nanocrystalline cobalt ferrite. *Jordan Journal of Physics* 2022; **15(1)**, 61-66.

[10] NP Prasetya, RI Setiyani, Utari, K Kusumandari, Y Iriani, J Safani, A Taufiq, NA Wibowo, S Suharno and B Purnama. Cation trivalent tune of crystalline structure and magnetic properties in coprecipitated cobalt ferrite nanoparticles. *Materials Research Express* 2023; **10(3)**, 036102.

[11] G Muscas, S Jovanović, M Vukomanović, M Spreitzer and D Peddis. Zn-doped cobalt ferrite: Tuning the interactions by chemical composition. *Journal of Alloys and Compounds* 2019; **796**, 203-209.

[12] PA Vinosha, A Manikandan, ASJ Ceicilia, A Dinesh, GF Nirmala, AC Preetha, Y Slimani, MA Almessiere, A Baykal and B Xavier. Review on recent advances of zinc substituted cobalt ferrite nanoparticles: Synthesis characterization and diverse applications. *Ceramics International* 2021; **47(8)**, 10512-10535.

[13] CJ Prabagar, S Anand, MA Janifer, S Pauline and PAS Theoder. Effect of metal substitution (Zn, Cu and Ag) in cobalt ferrite nanocrystallites for antibacterial activities. *Materials Today: Proceedings* 2021; **47**, 1999-2006.

[14] S Mandal and S Mukherjee. Magnetocaloric effect and critical behaviour in zinc doped cobalt ferrite nanoparticles. *Journal of Solid State Chemistry* 2023; **323**, 124008.

[15] HM Shashanka, S Saha, AJ Chelvane, B Sahoo and PN Anantharamaiah. Tuning magnetostrictive strain sensitivity through controlled spin-orbit and superexchange interactions: Nonmagnetic Zn and Mg cation substitution in $CoFe_2O_4$. *Journal of Materials Chemistry C* 2025; **13(22)**, 11060-11076.

[16] GV Duong, R Sato Turtelli, N Hanh, DV Linh, M Reissner, H Michor, J Fidler, G Wiesinger and R Grössinger. Magnetic properties of nanocrystalline $Co_{1-x}Zn_xFe_2O_4$ prepared by forced hydrolysis method. *Journal of Magnetism and Magnetic Materials* 2006; **307(2)**, 313-317.

[17] S Singhal, T Namgyal, S Bansal and K Chandra. Effect of Zn substitution on the magnetic properties of cobalt ferrite nano particles prepared via sol-gel route. *Journal of*

Electromagnetic Analysis and Applications 2010; **2(6)**, 376-381.

[18] TR Tatarchuk, ND Paliychuk, M Bououdina, B Al-Najar, M Pacia, W Macyk and A Shyichuk. Effect of cobalt substitution on structural, elastic, magnetic and optical properties of zinc ferrite nanoparticles. *Journal of Alloys and Compounds* 2018; **731**, 1256-1266.

[19] FM Zulhaina, S Nurjanah, U Utari, R Riyatun, S Suharno and B Purnama. Synthesis of zinc substituted cobalt ferrite nanoparticles by using sol-gel method as antibacterial material. *Key Engineering Materials* 2023; **941**, 207-214.

[20] N Tohluebaji, R Siri, N Muensit, C Putson, P Channuie, P Porrawatkul and J Yuennan. Hydrophobic and optical properties of P (VDF-HFP) nanofiber filled with nickel (II) chloride hexahydrate for dye-sensitized solar cells application. *Trends in Sciences* 2024; **21(9)**, 8762.

[21] M Hussain, A Mehmood, F Ali, ZA Sandhu, MA Raza, S Sajid, M Sohaib, MT Khan, AH Bhalli, A Hussain, MS Arshid, N Mehboob and AG Al-Sehemi. Tuning the magnetic behavior of zinc ferrite via cobalt substitution: A structural analysis. *ACS Omega* 2024; **9(2)**, 2536-2546.

[22] T Kusumaningsih, A Supriyanto, HB Akmal, FM Zulhaina, NP Prasetya and B Purnama. Nanoparticle- preparation- procedure tune of physical, antibacterial, and photocatalyst properties on silver substituted cobalt ferrite. *Results in Engineering* 2023; **18**, 101085.

[23] G Rajivgandhi, G Ramachandran, G Chackaravarthi, CK Chelliah, M Maruthupandy, F Quero, FA AL-mekhlafi, MA Wadaan and WJ Li. Preparation of antibacterial Zn and Ni substituted cobalt ferrite nanoparticles for efficient biofilm eradication. *Analytical Biochemistry* 2022; **653**, 114787.

[24] G Channagoudra, JPJ Nunez, RL Hadimani and V Dayal. Study of cation distribution in La^{3+} and Eu^{3+} substituted cobalt ferrite and its effect on magnetic properties. *Journal of Magnetism and Magnetic Materials* 2022; **559**, 169550.

[25] DR Lide. *CRC handbook of chemistry and physics.* CRC Press, Boca Raton, United States, 2005.

[26] VS Sharon, VK Haripriya, SS Nair, E Veena Gopalan, A George and KA Malini. Zinc-doped cobalt ferrite nanoparticles: Modified sol-gel synthesis, multifunctional properties, and cytotoxicity evaluation. *Journal of Sol-Gel Science and Technology* 2025; **114(1)**, 169-184.

[27] P Kumar, S Pathak, A Singh, K Jain, H Khanduri, L Wang, SK Kim and RP Pant. Observation of intrinsic fluorescence in cobalt ferrite magnetic nanoparticles by Mn^{2+} substitution and tuning the spin dynamics by cation distribution. *Journal of Materials Chemistry C* 2022; **10(35)**, 12652-12679.

[28] Suharyana, RR Febriani, NP Prasetya, Utari, NA Wibowo, Suharno, A Supriyanto, AH Ramelan and B Purnama. Sodium-hydroxide molarities influence the structural and magnetic properties of strontium-substituted cobalt ferrite nanoparticles produced via co-precipitation. *Kuwait Journal of Science* 2023; **50(4)**, 575-579.

[29] RD Waldron. Infrared spectra of ferrites. *Physical Review* 1955; **99(6)**, 1727.

[30] EH El-Ghazzawy and MA Amer. Structural, elastic and magnetic studies of the as-synthesized $Co_{1-x}Sr_xFe_2O_4$ nanoparticles. *Journal of Alloys and Compounds* 2017; **690**, 293-303.

[31] H Ghorbani, M Eshraghi, AA Sabouri Dodaran, P Kameli, S Protasowicki, C Johnson and D Vashaee. Effect of Yb doping on the structural and magnetic properties of cobalt ferrite nanoparticles. *Materials Research Bulletin* 2022; **147**, 111642.

[32] H Ghorbani, M Eshraghi and AA Sabouri Dodaran. Structural and magnetic properties of cobalt ferrite nanoparticles doped with cadmium. *Physica B: Condensed Matter* 2022; **634**, 413816.

[33] N Dhanda, P Thakur and A Thakur. Green synthesis of cobalt ferrite: a study of structural and optical properties. Materials Today: Proceedings 2023; **73**, 237-240.

[34] NP Prasetya, R Arilasita, H Aldila, NA Wibowo, Riyatun, Utari, Nuryani, T Tanaka and B Purnama. Single-domain configuration tune high coercive field in co-precipitated monazite-decorated cobalt ferrite nanoparticles. *Nano-Structures & Nano-Objects* 2024; **39**, 101301.

[35] D Djuhana, C Kurniawan, A Musadewi, NP Prasetya, Utari, Suharno, DH Kim and B Purnama. Impact of single domain configuration on photocatalytic dye removal in cerium-substituted cobalt ferrite nanoparticles. *Results in Physics* 2025; **76**, 108405.

[36] G Hussain, I Naz, F Ahmad, A Gyasi-Agyei and H Anwar. Insights into dysprosium-doped bismuth ferrite: A combined experimental and DFT study on structural, optical, and magnetic properties. *Physica B: Condensed Matter* 2025; **713**, 417361.

[37] S Ergin, K İçin, H Güngüneş and B Özçelik. Detailed studies on structural, morphological, optical, magnetic and mossbauer properties of Cu-substituted cobalt ferrite nanoparticles. *Physica Scripta* 2023; **98(3)**, 035807.

[38] W Tahir, T Zeeshan, S Waseem, MD Ali, Z Kayani, ZeH Aftab, SMT Mehtab and S Ezzine. Impact of silver substitution on the structural, magnetic, optical, and antibacterial properties of cobalt ferrite. *Scientific Reports* 2023; **13(1)**, 15730.

[39] M Liu, J Li, J Wang, H Yi, X Bao and X Gao. Effect of Mn and Zn binary co-substitution on structure and magnetic properties of cobalt ferrites. *Materials Science and Engineering: B* 2023; **289**, 116229.

[40] Sapna, N Budhiraja, V Kumar and SK Singh. Shape-controlled synthesis of superparamagnetic $ZnFe_2O_4$ hierarchical structures and their comparative structural, optical and magnetic properties. *Ceramics International* 2019; **45(1)**, 1067-1076.

[41] AM Bartashevich, SV Streltsov, EG Gerasimov, MA Semkin, AF Gubkin, AN Pirogov, NV Mushnikov, PB Terentev and MI Bartashevich. Commensurate magnetic structures in $ThCr_2Si_2$-type materials: A new symmetry-based classification scheme and prediction of emergent phenomena. *Materials Today Physics* 2025; **59**, 101905.